Correlation effects in the resonant Auger decay of the Xe $4d^{-1}_{3/2,5/2}6p$ states studied by high-resolution experiment and multiconfiguration Dirac-Fock theory

H. Aksela, O.-P. Sairanen, S. Aksela, A. Kivimäki, A. Naves de Brito, and E. Nõmmiste*
Department of Physics, University of Oulu, FIN-90570 Oulu, Finland,
and the Finnish Synchrotron Radiation Facility at Max-lab, Box 118, S-22100 Lund, Sweden

J. Tulkki
Optoelectronics Laboratory, Helsinki University of Technology, FIN-02150 Espoo, Finland

A. Ausmees,* S. J. Osborne, and S. Svensson
Department of Physics, Uppsala University, Box 530, S-751 21 Uppsala, Sweden
(Received 19 July 1994)

The deexcitation spectra of the resonantly excited Xe $4d^{-1}_{3/2,5/2}6p$ states have been recorded with very high photon and electron energy resolution using the new Finnish beam line at Max-lab, Lund, Sweden. The high resolution enables us to resolve the fine structures of the spectra by utilizing the Auger resonant Raman effect. By comparing the detailed intensity distribution of the $4d^{-1}_{3/2,5/2}6p \rightarrow 5p^{-2}6p$ transitions with the results of the single-channel multiconfiguration Dirac-Fock calculations, the strength of the configuration interaction in both the initial and final states of the resonant Auger decay is clarified. The probabilities of shake transitions are determined by both experiment and theory and the differences in the intensity distribution of spectator, shake, and normal Auger transitions are also discussed.

PACS number(s): 32.80.Hd, 32.80.Fb

I. INTRODUCTION

The resonant Auger spectra at the Kr $3d \rightarrow 5p$ and Xe $4d \rightarrow 6p$ resonances were reported for the first time by Eberhardt *et al.* [1]. Since then, the resonant Auger spectra of noble gases have been extensively studied both experimentally and theoretically [2–5]. With the exception of the high-resolution spectrum of Kr [5], the photon and the electron resolution were not sufficient to excite the various resonance states selectively and to resolve the detailed fine structures in the electron spectra. In a study on Xe published recently as a Rapid Communication [6] and completed in the present paper, both the photon and the electron energy resolution have been considerably improved. The narrow photon bandwidth has made it possible to carry out the measurements by utilizing the Auger resonant Raman effect, where the linewidths are not determined by the natural linewidth, but by the bandwidth of exciting radiation [7,8]. The advantage of high photon energy resolution is preserved by recording the resonant Auger spectra with a high-resolution electron spectrometer, which allows us to resolve the fine structures in detail.

In the resonant Auger spectrum the spectator electron in the initial and the final states of the decay couples with the electrons involved in the decay (referred to as the spectator-core coupling). The high resolution enables us to see how dramatic the changes are in the intensity distribution between the normal $4d^{-1} \rightarrow 5p^{-2}(^1S, ^1D, ^3P)$ and the resonant $4d^{-1}6p \rightarrow 5p^{-2}(^1S, ^1D, ^3P)6p$ Auger transitions in Xe. It is also possible to test whether theory is capable of reproducing the $^1S:^1D:^3P$ branching ratio correctly in both spectra. High-resolution spectra are of particular advantage in testing whether theory distributes the intensity correctly between the fine structures produced by the spectator-core coupling.

In a recent theoretical study [9], the intensity distributions and angular anisotropies of the Kr $3d^{-1}5p$ and Xe $4d^{-1}6p$ resonant Auger transitions were found to be very sensitive to the configuration interaction both in the initial ionic state (ISCI) and in the final ionic state (FISCI), as well as to the exchange effect and orbital relaxation. The changes in the relative intensities of the resonant Auger lines were found to be even stronger than the changes in the angular asymmetry parameters β calculated in various approximations. In this work we will compare the theoretical intensity distributions, obtained using different approximations, with each other and with our high-resolution experimental results. The comparison will be restricted to the resonant Auger transitions only. A preliminary comparison that was limited to the Xe $4d^{-1}_{5/2}6p$ resonant Auger decay and in particular to the transitions to the $5p^{-2}(^1D)6p$ final states has recently been presented as a Rapid Communication [6].

*Permanent address: Institute of Physics, Estonian Academy of Sciences, Riia 142, EE-2400 Tartu, Estonia.

The excited electron may not remain as a spectator electron during the Auger decay, but can shake to another orbital. The shake transitions have been observed in earlier studies [1–5] to play an important role in the deexcitation of the Ar $2p \rightarrow 4s, 3d$, Kr $3d \rightarrow 5p$, and Xe $4d \rightarrow 6p$ resonances. Now we can fully resolve from each other the Xe $4d^{-1}6p \rightarrow 5p^{-2}6p$ spectator transitions and the $4d^{-1}6p \rightarrow 5p^{-2}np$ shake transitions. This allows us to determine the relative contribution of the shake transitions and to compare them with the theoretical predictions.

The $5s$ photoelectron line accompanied by its correlation satellite structure, which results mainly from direct photoionization, also overlaps with the spectator and shake-up transitions. The $5s$-$5p$ satellite spectrum is dominated by the even-parity configurations $5p^{-2}ns$ and $5p^{-2}nd$, whereas the population of the odd-parity configurations $5p^{-2}np$ via direct photoionization is small. In contrast, the latter configuration is strongly populated through the resonance Auger decay. Since the $5p^{-2}ns$ and $5p^{-2}nd$ configurations have opposite parity as compared with the $5p^{-2}np$, the mixing via FISCI is not possible and the states with different parities can be treated independently. The excellent resolution enables a complete decomposition of the recorded spectrum according to the parity of the final state. Accurate determination of the intensity distribution between different decay channels is thus possible, which allows us to find out if the electron correlation is limited to the FISCI only.

This paper is organized as follows. In the next section we describe the measurements and experimental results. The computational approximations and the results of calculations are described in Sec. III. A comparison between experiment and theory is presented in Sec. IV.

II. EXPERIMENT

A. Measurements

The measurements were performed at the Finnish beam line (BL 51) at Max-laboratory in Lund, Sweden. A detailed description of the beam line has been published elsewhere [10]. Briefly, the beam line uses synchrotron radiation from an undulator in the photon energy range of 60–600 eV and it has a modified SX-700 plane grating monochromator [11] with a plane elliptical focusing mirror. The beam line contains a permanent differential pumping section designed to isolate effectively high-pressure gas experiments from the ultrahigh vacuum of the monochromator. This section includes also a toroidal refocusing mirror in order to get a small spot size ($\varnothing \approx 1$ mm) in the experimental station.

The electron spectrometer SES-144 [12] has a hemispherical electron analyzer. The analyzer is provided with a four-element retarding electron lens that focuses the electrons onto the entrance slit of the analyzer. The detector is a standard microchannel plate detector from Galileo Corp. Detected electron pulses are accelerated onto a fluorescent screen and the resulting optical flashes are scanned using a charge coupled device television camera. A very effective differential pumping is achieved by cutting holes in the lens elements and using the electron lens itself as a pumping stage. The pressure in the sample compartment is on the order of 10^{-3}–10^{-4} mbar. The optimum resolution of the electron spectrometer at a 10-eV pass energy is about 40 meV.

The degree of linear polarization of undulator radiation in the case of lower-order harmonics has been shown to be very high [13,14]. In the case of practically complete linearly polarized radiation, the angle-dependent photoemission is a function of the angle between the electric field vector and the spectrometer opening only. Our instrument has been mounted with the principal axis of the electron lens in the pseudomagic angle of 54.7° versus the horizontal plane, which allows direct angular independent measurements of the branching ratios. An almost complete absence of higher-order contributions in the exciting radiation enables the detection of pure resonant Auger spectra free from normal Auger electron lines, as well as from additional photoelectron lines and their satellites.

The photon energy was set to match the maximum of the resonance energy ($4d_{5/2} \rightarrow 6p$, 65.110 eV; $4d_{3/2} \rightarrow 6p$, 67.039 eV [15]). The monochromator exit slit size of 10 μm used in this study results in photon energy resolution of about 8 meV at $h\nu = 65$ eV. Thus the photon bandwidth is much narrower than the estimated lifetime widths 110–120 meV [15] of the $4d^{-1}_{5/2,3/2}6p$ excited states and therefore we recorded the spectra in the Auger resonant Raman mode. The total width of the resonant Auger lines is less than 50 meV, resulting mainly from the spectrometer broadening. This kind of resolution is necessary when studying the finest details in the spectra.

B. Experimental results

The deexcitation spectra of the resonantly excited Xe $4d^{-1}6p$ states are presented in Fig. 1. The kinetic energy calibration has been done with the aid of the photoexcitation energies [15] for the initial states and optical energies [16] for the final states of the resonant Auger transitions. The spectra have been corrected for the spectrometer transmission by using an experimentally determined correction function [17].

In Figs. 2–7 the energy range of the resonant Auger transitions is shown in more detail. The energies and intensities of the peaks were determined by using a least-squares fit of Voigt functions. The energy separation of the resonant Auger lines was taken from the energy splitting of the final state levels determined by optical measurements [16] and was kept fixed during the fitting procedure. The linewidths were also kept fixed after they had been determined from strong, well separable lines. In both spectra the linewidths for the transitions to the even-parity final states were obtained from the $5s^{-1}$ photoelectron line (No. 1 in Fig. 2). In the $4d^{-1}_{5/2}6p$ deexcitation spectrum, the linewidth for the transitions to the resonantly enhanced odd-parity final states was obtained from the $4d^{-1}_{5/2}6p \rightarrow 5p^{-2}(^3P)6p(^2P_{3/2})$ resonant Auger line (No. 26 in Fig. 3, upper part). In the $4d^{-1}_{3/2}6p$ de-

excitation spectrum the corresponding linewidth was obtained from the $4d_{3/2}^{-1}6p \rightarrow 5p^{-2}(^1D)6p(^2F_{5/2})$ resonant Auger line (No. 39 in Fig. 4, lower part). The fit of those lines gave full width at half maximum (FWHM) values of 46 meV ($4d_{5/2}^{-1}6p$ spectrum) and 47 meV ($4d_{3/2}^{-1}6p$ spectrum) for the $5s^{-1}$ photoelectron line and its correlation satellites and 43 meV ($4d_{5/2}^{-1}6p$ spectrum) and 45 meV ($4d_{3/2}^{-1}6p$ spectrum) for the resonant Auger lines. The small difference in the linewidths between the two spectra is most probably caused by small changes in the experimental conditions.

The fitting results are presented in Tables I and II. The assignment of the final states is based on the optical data from Hansen and Persson [16] and in the case of the $5p^{-2}6p$ states on the results of calculations described in Sec. III. Also a photoelectron spectrum measured at 60-eV photon energy as well as the results of Carlsson-Göthe *et al.* [18] were used to assign the correlation satellites. The shake transitions $4d^{-1}6p \rightarrow 5p^{-2}np$ ($n = 7, 8$) were determined by using the deexcitation spectra of $4d^{-1}7p$ and $4d^{-1}8p$ resonantly excited states. The photoelectron spectrum, along with the decay spectra taken at higher resonances, will be published later.

By comparing the deexcitation spectra with the pure photoelectron spectrum [18] we see that most of the population of the $5p^{-2}6p$ odd-parity final states originates from the spectator decay. The contribution of the direct photoionization to these final states is, in general, very small. In the $4d_{5/2}^{-1}6p \rightarrow 5p^{-2}6p$ deexcitation spectrum, only the $5p^{-2}(^1D)6p(^2F_{5/2})$ final state (line 39 in Fig. 4) is considerably populated via the direct photoionization. In the $4d_{3/2}^{-1}6p \rightarrow 5p^{-2}6p$ spectrum the transitions to the final states $5p^{-2}(^3P)6p(^2P_{3/2}, {}^4D_{3/2}$, and $^4D_{1/2})$ (lines 26, 34, and 36 in Fig. 3) have intensities comparable to those in the photoelectron spectrum. In addition to the spectator transitions, the peaks associated with the $5p^{-2}7p$ odd-parity final states (lines 53–56, 64, 66, 70–73, 79–85, 88–93, 109, and 110) also show clear enhancement indicating significant shake-up contribution.

The lines associated with the even-parity final states ($5s$ correlation satellites) have in most cases roughly the same intensity in the deexcitation spectra as in the photoelectron spectrum. A very exact comparison is difficult to make since the intensities are usually quite small and the relative uncertainties in the fitting results become bigger due to moderate statistics. The He II α excited photoelectron spectrum of Carlsson-Göthe *et al.* [18] has also satellite lines originating from excitation by other radiation components than the main line and these satel-

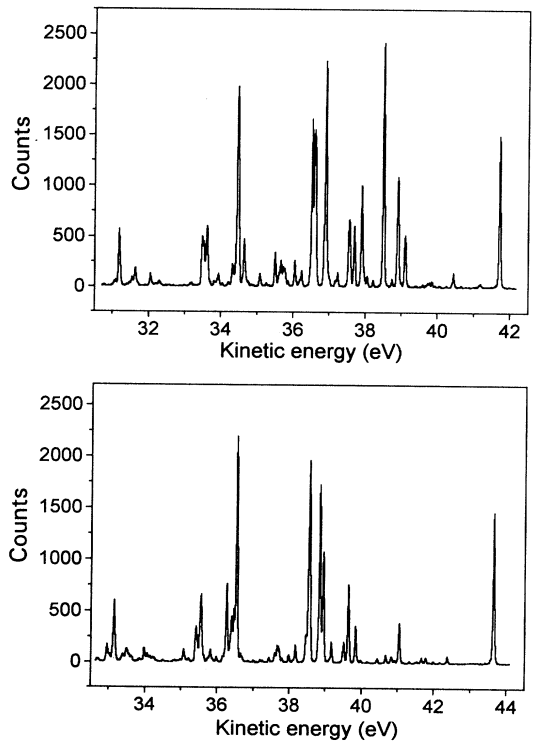

FIG. 1. Upper part: the electron spectrum of Xe excited by 65.11-eV photons corresponding to the $4d_{5/2}^{-1}6p$ resonant excitation. Lower part: the electron spectrum of Xe excited by 67.039-eV photons corresponding to the $4d_{3/2}^{-1}6p$ resonant excitation.

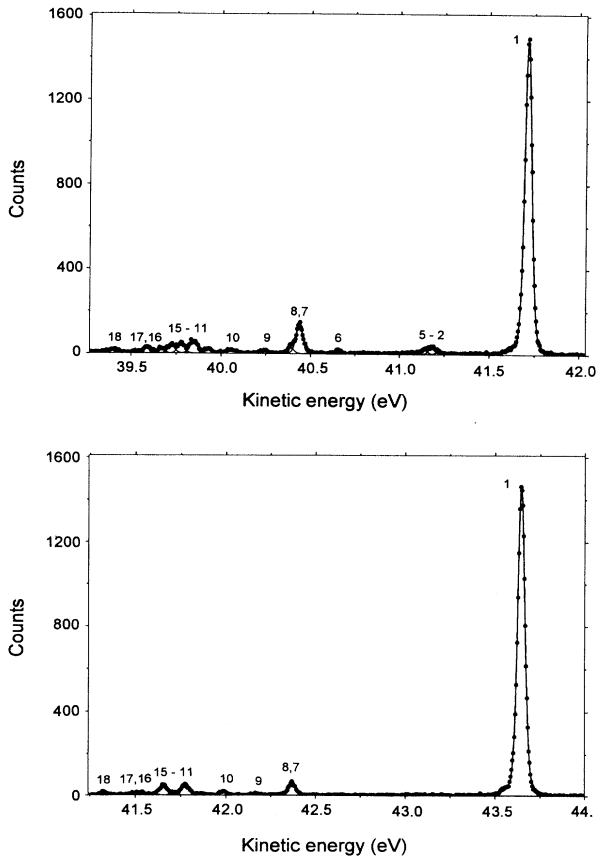

FIG. 2. The kinetic energy region of lines 1–18 (in Table I) of the electron spectrum of Xe excited by 65.110-eV photons (upper part) and 67.039-eV photons (lower part). The solid line represents the least-squares fit of Voigt functions to the experimental points.

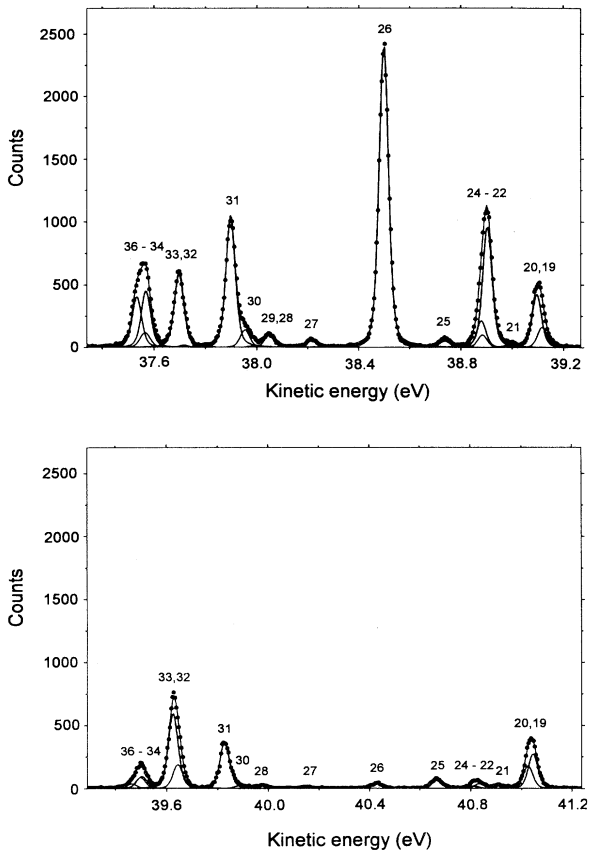

FIG. 3. Kinetic energy region of lines 19–36 in Table I. For details see the caption of Fig. 2.

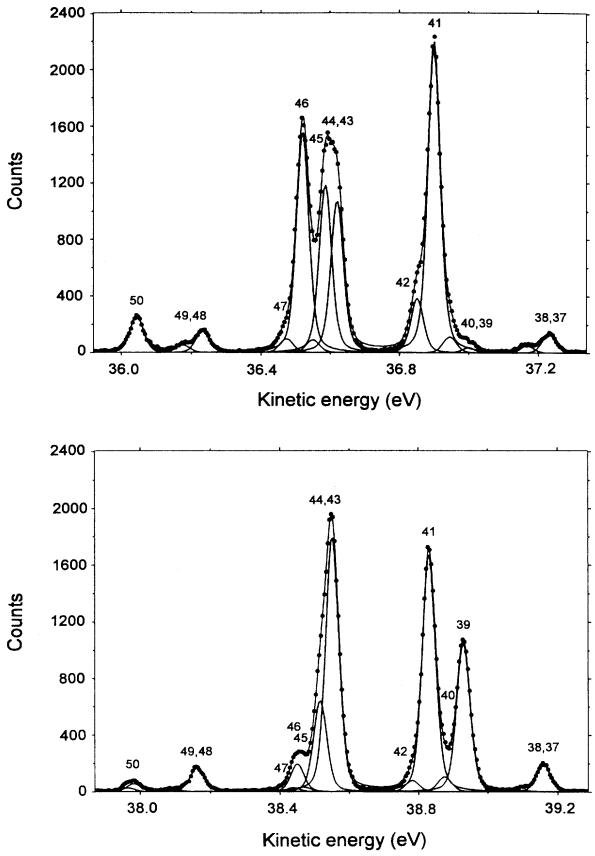

FIG. 4. Kinetic energy region of lines 37–50 in Table I. For details see the caption of Fig. 2.

lites make the comparison of intensities difficult in some cases. However, a few notes can be made. In both deexcitation spectra, the lines associated with the final states $5p^{-2}(^1S)6s(^2S_{1/2})$ and $5p^{-2}(^1D)5d(^2S_{1/2})$ (lines 40 and 48 in Fig. 4) show clear enhancement. Moreover, the transitions to the close lying states $5p^{-2}(^1D)5d(^2P_{1/2}$ and $^2D_{3/2})$ (lines 37 and 38) seem to exchange intensities compared to the results of [18]. It is difficult to say whether it is a real effect or just some error in the fitting of the photoelectron spectrum. The decay of the $4d_{5/2}^{-1}6p$ excited states gives clearly more intensity also to the transitions to the $5p^{-2}(^3P)6s(^4P_{1/2})$, $5p^{-2}(^3P)6d(^2P_{1/2}$, $^2F_{7/2})$, and $5p^{-2}(^1S)5d(^2D_{5/2})$ as well as $5p^{-2}(^3P)6d(^4F_{5/2})$ states (lines 7, 50, and 59). On the other hand, the transitions to the $5p^{-2}(^1D)5d(^2G_{9/2}$, $^2G_{7/2})$ states (line 25) in the $4d_{5/2}^{-1}6p \rightarrow 5p^{-2}6p$ decay and to the $5p^{-2}(^1D)5d(^2F_{5/2})$ state (line 27) in the $4d_{3/2}^{-1}6p \rightarrow 5p^{-2}6p$ decay seem to lose intensity compared to the results of [18]. On the whole, the changes are rather small.

III. CALCULATIONS

A. Computational method

The transition rates of the resonant Auger processes were calculated using a computer code, which is based on a single-channel multiconfiguration Dirac-Fock (MCDF) method, described in [19,20]. The approach was recently used to obtain the angular asymmetries of the Xe $4d^{-1}6p \rightarrow 5p^{-2}6p$ transitions [9] and the reader is referred to that reference for further details. Here we will present only a short summary of the actual calculations.

In all calculations, the initial and final states of the atom (ion) were described by multiconfiguration wave functions accounting for the initial and final state configuration interaction [21]. For the initial state we included three jj-coupled configurations $4d_{5/2}^{-1}6p_{3/2}, J = 1$; $4d_{3/2}^{-1}6p_{1/2}, J = 1$; and $4d_{3/2}^{-1}6p_{3/2}, J = 1$. For the final ionic state all the jj-coupled configurations, resulting from the nonrelativistic configurations $5s^{-2}6p, 5s^{-1}5p^{-1}6p, 5p^{-2}6p$, $5s^{-1}$, and $5p^{-1}$, were included. The continuum orbital was optimized in a jj-average field of the core plus spectator electron and made orthogonal to the bound orbitals by Lagrangian multipliers [9].

The effects of the choice of orbitals and exchange were studied by calculating the resonant Auger spectra in the following approximations.

FE: In this approach the bound orbitals were optimized for the final ionic state. Also the mixing coefficients appearing in the initial state multiconfiguration wave function were calculated by using final state orbitals in the diagonalization of the initial state Hamiltonian. The ex-

change interaction between the continuum and core electrons was fully taken into account.

F: This approximation is identical to FE, except that the exchange interaction was not included in the calculation of the continuum orbital. Accordingly, the difference between FE and F indicates the effect of exchange interaction.

IE: In this approximation the bound orbitals optimized for the initial excited atomic state were also used in the final state wave function. In analogy to FE, the final ionic state mixing coefficients were determined by using the initial state orbitals and the exchange was included for the continuum electron.

FEI: This approximation is equivalent to FE, except that the initial state mixing coefficients were obtained from the initial state self-consistent-field (SCF) calculation. This approach does not conserve the orthogonality of many-electron wave functions exactly, but only uses a different orbital basis in the calculation of initial and final state mixing coefficients, which means that some contribution from relaxation is included.

FE0: This approximation is identical to FE, except that the ISCI was completely omitted.

B. Results of calculations for the $4d^{-1}_{3/2,5/2}6p \rightarrow 5p^{-2}6p$ spectator Auger transitions

The resonance excitation of the $4d$ electron, at the photon energies of this experiment, populates three atomic states mixed from the jj-coupled $4d^{-1}_{3/2,5/2}6p_{1/2,3/2}, J = 1$ configurations, according to the dipole selection rules. These three photoexcited atomic states (referred to A, B, and C hereafter) that are the initial states of the subsequent Auger decay have different characters. The first resonance state A, separated by 1.97 eV from the next one (according to the initial state SCF calculations), is mainly due to the $4d^{-1}_{5/2}6p_{3/2}, J = 1$ configuration with only a weak mixing with the $4d^{-1}_{3/2}6p_{1/2}, J = 1$ and the $4d^{-1}_{3/2}6p_{3/2}, J = 1$ configurations. The Auger transitions originating from this state A, since they are free from the initial state effects, are well suited to study the sensitivity of the relative intensities to the exchange, relaxation, and FISCI (see the results of the F, FE, and IE calculations in Table III).

The next two resonances B and C, which involve a strong mixing between the $4d^{-1}_{3/2}6p_{1/2}, J = 1$ and $4d^{-1}_{3/2}6p_{3/2}, J = 1$ configurations, cannot be excited selectively because their energy splitting is small (5.5 meV predicted by the initial state SCF calculations) as com-

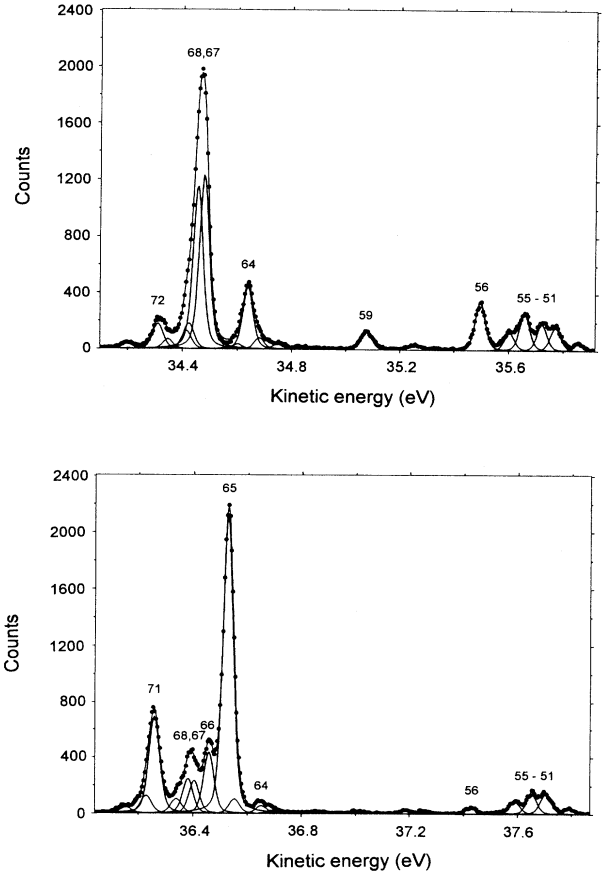

FIG. 5. Kinetic energy region of lines 51–73 in Table I. For details see the caption of Fig. 2.

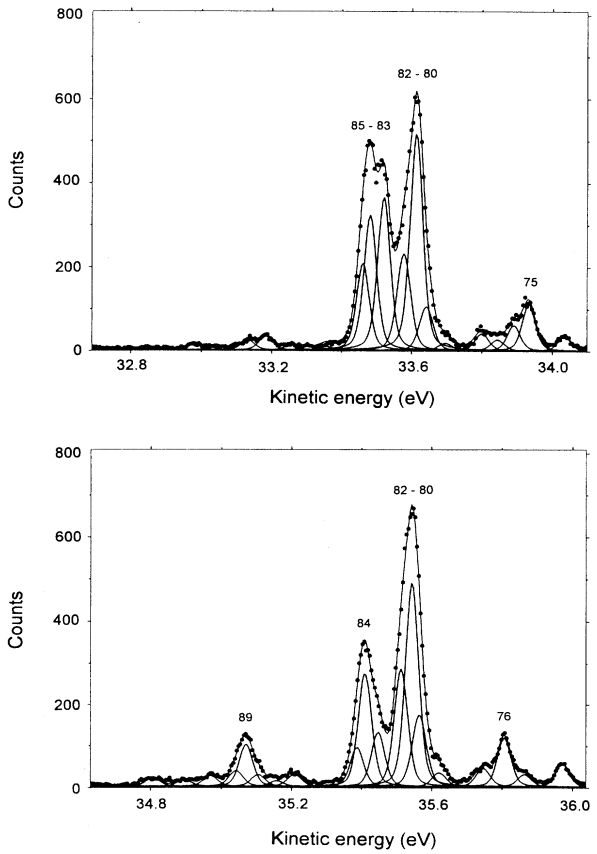

FIG. 6. Kinetic energy region of lines 74–93 in Table I. For details see the caption of Fig. 2.

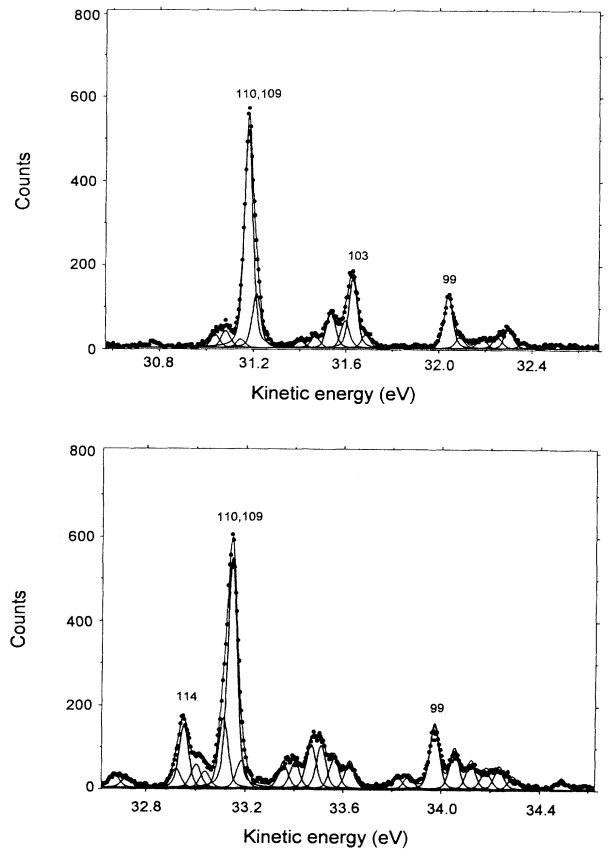

FIG. 7. Kinetic energy region of lines 93–117 in Table I. For details see the caption of Fig. 2.

pared with the photon bandwidth (8 meV), but they are excited simultaneously with a population ratio that is governed by the photoexcitation probability. Therefore, the calculated $4d_{3/2}^{-1}6p$ resonant Auger spectrum has to be constructed as a proper average by using the MCDF photoexcitation probabilities as weights for the partial Auger rates [9]. In a calculation using the GRASP computer code [21], a photoexcitation branching ratio of 287 was obtained, which indicates that the spectrum from the initial atomic state B gives the dominant contribution to the $4d_{3/2}^{-1}6p$ resonant Auger spectrum. The prediction for the photoexcitation branching ratio plays an important role when the theory is compared with experiment because the Auger intensity distributions of the two initial states B and C differ remarkably from each other (see Table IV). The difference is due to the heavy mixing of the jj-coupled $4d_{3/2}^{-1}6p_{1/2,3/2}, J = 1$ configurations which, furthermore, depends strongly on the choice of the basis set. This can be seen from the partial transition rates obtained in the FE, FEI, and FE0 approximations (Table IV) for the two initial states B and C. In summary, the $4d_{3/2}^{-1}6p$ transitions offer an excellent possibility to investigate the influence of the initial state effects on the intensity distribution.

The ΔE_{SCF} energies, obtained as the difference between the initial and final state SCF energies, are given in Table III for the $4d_{5/2}^{-1}6p$ transitions. The energetic order of the levels and the magnitude of their splitting was found to change dramatically when predicted by final or initial state orbitals. The mixing of final state wave functions was different in the two cases and altered some assignments based on the LS symbols. The LS symbols given in the tables are the leading LS terms from a calculation with the final state orbital set. Due to a large mixing of the states, the symbols should be considered only as a tag for the final state. The symbols used may differ from those used earlier in the literature; but this does not mean any reassignment of lines, but only indicates the sensitivity of the FISCI to the orbital set.

1. *The $4d_{5/2}^{-1}6p_{3/2}$ spectator Auger transitions: A comparison of calculated results*

The overall intensity distributions of the $4d_{5/2}^{-1}6p_{3/2} \rightarrow 5p^{-2}6p$ transitions are similar in the F, FE, and IE approximations, as shown in Table III. The approximation F seems to predict larger partial transition rates than FE or IE for all the transitions, except for the transitions to the $5p^{-2}(^1D)6p(^2F_{7/2})$ state, the rate of which shows a clear increase relative to the others when the exchange is included. Because of the low kinetic energy, the exchange potential becomes important in the effective potential seen by the Auger electron. This reflects in the changes of the branching ratios, even though the effect is not large in most cases. Instead, the exchange effect has a large influence on the total transition rates. This is demonstrated by the fact that the calculated half widths of the initial state were 0.289 eV and 0.192 eV in the F and FE approximations, respectively. Both approximations overestimate the experiment (0.111 eV), but the omission of the exchange interaction results in the most dramatic discrepancy with experiment. Note that the total transition rate contains the partial rates of the transitions to the $5s^{-2}6p$, $5s^{-1}5p^{-1}6p$, $5p^{-2}6p$, $5s^{-1}$, and $5p^{-1}$ final states, but only the partial rates of the $4d^{-1}6p \rightarrow 5p^{-2}6p$ transitions are given in Table III.

The partial rates of several transitions, particularly those to the states with $J = 1/2, 3/2$, were found to depend strongly on the mixing of the final state configurations. Furthermore, the FISCI is extremely sensitive to the one-electron orbitals, as can be seen by comparing the FE and IE results in Table III with each other. The initial state effect is negligible in the case of the $4d_{5/2}^{-1}6p_{3/2}$ resonant Auger decay, which is why the FE and FEI (not shown) results are identical.

Table III also displays the results reported by Chen [22]. Similar results were also given by Fritzsche [23]. Both authors generated the continuum waves in the local potential of the final ionic state neglecting the exchange with bound electrons and also included a more limited configuration basis in the calculation of FISCI. Their results are quite close to our F results, but differ from our other results, which is easy to understand since their method closely resembles our F approximation.

The combined effect of exchange and orbital relax-

ation, the latter one manifesting itself as distinct changes in the FISCI, can thus be concluded to be of great importance in the $4d_{5/2}^{-1}6p_{3/2}$ resonant Auger decay of Xe. The changes in the relative transition rates are much larger between the FE and IE results than between the F and FE, which indicates that the FISCI plays a more prominent role in branching ratios than the exchange. Instead, the choice of the orbital set has a minor influence (about 13%) on the total transition rates.

2. The $4d_{3/2}^{-1}6p_{1/2,3/2}$ spectator Auger transitions: A comparison of calculated results

The two $4d_{3/2}^{-1}6p_{1/2,3/2}, J = 1$ jj-coupled initial states are strongly mixed according to the calculations, the mix-

TABLE I. Energies (in eV) and intensities of the observed lines in the measured electron spectrum of Xe after $4d_{5/2}^{-1}6p$ resonant excitation (65.110 eV) and $4d_{3/2}^{-1}6p$ resonant excitation (67.039 eV). Intensities are normalized relative to the $5s^{-1}$ photoelectron line, the uncertainty being less than 5 units in the last digit for values below 10 and less than 2 units for values above 10. The listed term is the leading LS term. The photoelectron results were taken from Ref. [18].

Term	Line No.	$4d_{5/2}^{-1}6p$ Energy	$4d_{5/2}^{-1}6p$ Intensity	$4d_{3/2}^{-1}6p$ Energy	$4d_{3/2}^{-1}6p$ Intensity	Photoelectron
$5s^{-1}\ ^2S_{1/2}$	1	41.717	100	43.647	100	100
$(^3P)6s^2P_{3/2}$	2	41.221	0.9			0.8
$(^3P)5d^4D_{5/2}$	3	41.183	2.1			0.5
$(^3P)5d^4D_{7/2}$	4	41.140	1.6			0.1
$(^3P)5d^4D_{3/2}$	5	41.061	0.9			0.6
$(^3P)5d^4F_{9/2}$	6	40.657	1.3			0.7
$(^3P)6s^4P_{1/2}$	7	40.441	9.2	42.370	4.2	2.4
$(^3P)5d^2F_{7/2}$	8	40.390	1.9	42.310	0.3	1.4
$(^3P)6s^4P_{3/2}$	9	40.237	1.2	42.169	0.7	0.4
$(^3P)5d^2P_{1/2}$	10	40.056	1.4	41.988	1.4	0.4
$(^3P)5d^2D_{3/2}$	11	39.928	1.5	41.859	0.5	0.9
$(^3P)5d^4P_{1/2}$	12	39.848	4.1	41.776	3.6	4.0
$(^3P)5d^4F_{5/2}$	13	39.779	3.0	41.708	0.5	3.0
$(^3P)6s^2P_{1/2}$	14	39.724	2.5	41.655	3.4	1.7
$(^3P)5d^4F_{3/2}$	15	39.667	1.4	41.611	0.3	
$(^3P)5d^4P_{5/2,3/2}$	16	39.590	2.0	41.532	0.8	1.0
$(^3P)5d^4F_{7/2}$	17	39.521	0.7	41.487	0.6	
$(^1D)6s^2D_{5/2}$	18	39.399	1.5	41.325	1.1	1.3
$(^3P)6p^4P_{3/2}$	19	39.119	11	41.048	17	0.6
$(^3P)6p^4P_{5/2}$	20	39.098	27	41.028	12	
$(^1D)6s^2D_{3/2}$	21	38.975	1.1	40.908	1.6	1.0
$(^3P)6p^2D_{5/2}$	22	38.906	63	40.835	2.5	
$(^3P)6p^2S_{1/2}$	23	38.886	6.6	40.815	1.3	0.6
$(^3P)6p^4D_{7/2}$	24	38.882	14	40.811	1.1	
$(^1D)5d^2G_{9/2,7/2}$	25	38.739	3.7	40.667	5.3	12
$(^3P)6p^2P_{3/2}$	26	38.501	156	40.430	2.8	2.0
$(^1D)5d^2F_{5/2}$	27	38.216	3.7	40.149	0.8	5.9
$(^3P)6p^2P_{1/2}$	28	38.050	6.3	39.979	1.5	0.4
$(^3P)5d^2F_{7/2}$	29	37.988	0.9			0.8
$(^3P)6p^4P_{1/2}$	30	37.955	9.2	39.884	1.4	
$(^3P)6p^2D_{3/2}$	31	37.899	67	39.829	24	0.7
$(^3P)6p^4D_{5/2}$	32	37.716	1.3	39.645	12	0.9
$(^3P)6p^4S_{3/2}$	33	37.698	38	39.627	38	
$(^3P)6p^4D_{3/2}$	34	37.570	29	39.499	5.7	
$(^3P)5d^2D_{5/2}$	35	37.567	8.0	39.504	6.5	30
$(^3P)6p^4D_{1/2}$	36	37.535	26	39.464	2.4	
$(^1D)5d^2P_{1/2}$	37	37.232	9.0	39.161	13	1.1
$(^1D)5d^2D_{3/2}$	38	37.169	3.7	39.102	0.8	17
$(^1D)6p^2F_{5/2}$	39	37.001	2.6	38.931	68	1.0
$(^1S)6s^2S_{1/2}$	40	36.947	7.7	38.877	7.2	1.7
$(^1D)6p^2P_{3/2}$	41	36.902	139	38.832	108	3.0
$(^1D)6p^2F_{7/2}$	42	36.853	25	38.783	5.2	1.1
$(^1D)6p^2D_{3/2}$	43	36.621	70	38.552	116	0.8
$(^1D)6p^2D_{5/2}$	44	36.587	77	38.517	41	
$(^3P)7s^4P_{5/2}$	45	36.550	6.2	38.471	2.2	3.8
$(^1D)6p^2P_{1/2}$	46	36.521	102	38.451	13	
$(^3P)7s^2P_{3/2}$	47	36.474	6.7	38.438	1.9	
$(^1D)5d^2S_{1/2}$	48	36.232	10	38.162	11	He sat.
$(^3P)6d^4D_{7/2,5/2}$	49	36.175	3.8	38.095	1.1	
$(^3P)6d^2P_{1/2},\ ^2F_{7/2}$				37.982		
$(^1S)5d^2D_{5/2}$	50	36.045	17	37.964	5.5	5.0
$(^1S)5d^2D_{3/2}$	51	35.858	3.2	37.792	2.4	
$(^3P)6d^4P_{1/2}$	52	35.774	11	37.706	9.4	10
$(^3P)7p^4D_{3/2,5/2}$	53	35.724	12	37.654	9.1	
$(^3P)7p^4P_{5/2}$	54	35.661	17	37.592	5.5	9.6
$(^3P)7p^4P_{1/2}$	55	35.606	8.4	37.540	0.8	
$(^3P)7p^4P_{3/2}$	56	35.498	22	37.430	2.9	1.1
$(^3P)7s^4P_{3/2}$	57			37.255	1.3	He sat.
$(^3P)7s^2P_{1/2}$	58	35.254	2.5	37.186	1.5	He sat.
$(^3P)6d^4F_{5/2}$	59	35.078	9.2	37.010	1.1	1.3
$(^3P)6d^4F_{7/2}$	60			36.858	0.8	He sat.
$(^3P)6d^2F_{5/2}$	61	34.749	2.5	36.692	1.6	
$(^3P)8s^4P_{5/2}$	62			36.652	3.8	2.1
$(^3P)8s^2P_{3/2}$	63	34.682	5.3			
$(^3P)7p$	64	34.640	29	36.553	6.6	He sat.
$(^1S)6p^2P_{1/2}$	65	34.602	2.4	36.528	137	He sat.
$(^3P)7p, 4f$	66			36.459	28	
$(^1S)6p^2P_{3/2}$	67	34.479	80	36.405	15	4.0
-"-	68	34.456	75	36.382	16	
$(^1D)7s^2D_{5/2}$	69	34.424	12	36.339	7.0	
$(^3P)7p$	70	34.415	8.4			
$(^3P)7p$	71	34.348	4.6	36.259	47	
$(^3P)7p$	72	34.312	12	36.229	8.5	
$(^3P)7p$	73	34.200	2.5	36.154	2.9	
$(^1D)6d^2G_{7/2,9/2}$	74	34.035	2.2	35.973	3.4	2.4
$(^1D)6d^2P_{3/2},\ ^2F_{5/2}$	75	33.934	7.2	35.864	1.9	He sat.
$(^1D)6d^2D_{5/2},\ ^2F_{7/2}$	76	33.892	3.9	35.808	7.5	He sat.
$(^1D)6d^2P_{1/2}$	77	33.846	1.7	35.761	1.4	5.1
$(^1D)6d^2D_{3/2}$	78	33.802	2.7	35.736	1.8	
$(^1D)7p, 4f$	79	33.697	1.2	35.622	2.2	2.4
$(^1D)7p, 4f$	80	33.643	7.0	35.566	12	0.4
$(^1D)7p, 4f$	81	33.614	33	35.545	31	
$(^1D)7p, 4f$	82	33.579	15	35.514	18	
$(^1D)7p, 4f$	83	33.522	24	35.448	8.4	11
$(^1D)7p, 4f$	84	33.483	21	35.411	18	
$(^1D)7p, 4f$	85	33.462	14	35.388	6.0	
$(^3P)5g, 7g$	86	33.357	0.6	35.208	2.0	5.4
$(^3P)5g, 7g$	87	33.256	0.8	35.158	1.9	
$(^1D)7p, 4f$	88	33.184	2.2	35.105	1.9	
$(^1D)7p, 4f$	89	33.132	1.6	35.071	6.5	
$(^1D)7p, 4f$	90			35.042	2.4	
$(^1D)7p, 4f$	91	33.042	0.7	34.969	1.8	
$(^1D)7p, 4f$	92	32.978	1.1	34.895	1.1	
$(^1D)7p, 4f$	93			34.806	1.4	
	94	32.365	0.9	34.295	1.7	
$(^1S)7s^2S_{1/2}$	95	32.304	3.2	34.238	3.3	5.0
	96	32.254	2.0	34.185	2.9	
	97	32.188	1.7	34.124	4.0	
	98	32.094	1.9	34.057	5.9	
	99	32.044	8.4	33.976	10	
	100			33.871	1.8	1.7
	101			33.823	2.0	
	102	31.687	2.2	33.629	3.9	1.3
	103	31.633	11	33.565	4.7	
	104	31.599	4.3	33.512	6.6	
	105	31.537	5.8	33.471	7.1	3.8
	106	31.469	2.0	33.405	4.1	2.4
	107	31.404	1.2	33.359	3.7	
	108			33.186	4.2	
$(^1S)7p$	109	31.216	8.5	33.148	35	
$(^1S)7p$	110	31.181	34	33.113	11	
	111	31.147	1.4			
	112			33.039	2.6	1.9
	113	31.084	2.8	33.003	3.8	
	114	31.039	2.1	32.954	9.4	
	115			32.922	2.9	
	116	30.773	1.0	32.722	1.5	1.7
	117			32.673	2.0	

TABLE II. Experimental energies and intensities of the Xe $4d^{-1}6p \rightarrow 5p^{-2}6p$ resonant Auger lines. Intensities are given as percentages of the total intensity. The listed terms are leading LS terms.

Final ionic state			$4d_{5/2}^{-1}6p$		$4d_{3/2}^{-1}6p$	
Parent	Term	Line No.	Energy (eV)	Intensity (%)	Energy (eV)	Intensity (%)
$5p^{-2}(^3P)6p$	$^4P_{3/2}$	19	39.12	1.03	41.05	2.72
	$^4P_{5/2}$	20	39.10	2.66	41.03	1.80
	$^2D_{5/2}$	22	38.91	6.09	40.84	0.38
	$^2S_{1/2}$	23	38.89	0.65	40.82	0.21
	$^4D_{7/2}$	24	38.88	1.36	40.81	0.16
	$^2P_{3/2}$	26	38.50	15.2	40.43	0.43
	$^2P_{1/2}$	28	38.05	0.62	39.98	0.24
	$^4P_{1/2}$	30	37.96	0.90	39.88	0.22
	$^2D_{3/2}$	31	37.90	6.57	39.83	3.67
	$^4D_{5/2}$	32	37.72	0.13	39.65	1.92
	$^4S_{3/2}$	33	37.70	3.70	39.63	5.96
	$^4D_{3/2}$	34	37.57	2.84	39.50	0.88
	$^4D_{1/2}$	36	37.54	2.54	39.46	0.37
$5p^{-2}(^1D)6p$	$^2F_{5/2}$	39	37.00	0.25	38.93	10.6
	$^2P_{3/2}$	41	36.90	13.6	38.83	16.9
	$^2F_{7/2}$	42	36.85	2.44	38.78	0.81
	$^2D_{3/2}$	43	36.62	6.79	38.55	18.1
	$^2D_{5/2}$	44	36.59	7.48	38.52	6.47
	$^2P_{1/2}$	46	36.52	9.88	38.45	1.96
$5p^{-2}(^1S)6p$	$^2P_{1/2}$	65	34.60	0.24	36.53	21.4
	$^2P_{3/2}$	67	34.48	7.76	36.41	2.34
	$^2P_{3/2}$	68	34.46	7.28	36.38	2.47

ing being extremely sensitive to the basis set. The FE and FEI results in Table IV demonstrate the influence of the basis set to the ISCI. The changes in the intensity distribution are dramatic in passing from the FE to the FEI approximation and are often opposite for the two initial atomic states B and C. The two results also differ distinctively from the lowest level approximation FE0 where the ISCI is completely omitted. The branching ratio of the doublet due to the transitions to the $5p^{-2}(^1D)6p(^2F_{5/2}$ and $^2F_{7/2})$ final states seems to be the most sensitive to the ISCI.

The two initial states B and C given in Table IV are simultaneously excited with the population ratio determined by the photoexcitation probabilities. Thus the photoexcitation branching ratio remarkably influences the spectral structure. A photoexcitation branching ratio

TABLE III. Calculated energies and intensities (without multiplication by overlap integrals) for Xe $4d_{5/2}^{-1}6p$ Auger transitions. F indicates single-channel results obtained using final state orbitals and excluding the exchange for the continuum electron. ISCI was computed using final state orbitals. FE is the same as F but the exchange was included. IE indicates single-channel values obtained using initial state orbitals with exchange. FISCI was calculated using initial state orbitals. The listed term is the leading LS term, which, due to a large mixing of the states, should be considered only as a tag of the transition.

Final ionic state		Line	Energy (eV)		Intensity (10^{-3} a.u.)			
Parent	Term	No.	Calc.	Expt.	F	FE	IE	Chen[a]
$5p^{-2}(^3P)6p$	$^4P_{3/2}$	19	39.86	39.12	0.025	0.012	0.003	0.016
	$^4P_{5/2}$	20	39.86	39.10	0.126	0.056	0.032	0.121
	$^2D_{5/2}$	22	39.64	38.91	0.176	0.080	0.117	0.169
	$^2S_{1/2}$	23	39.60	38.89	0.020	0.015	0.019	0.025
	$^4D_{7/2}$	24	39.64	38.88	0.052	0.043	0.038	0.047
	$^2P_{3/2}$	26	39.16	38.50	0.360	0.158	0.215	0.452
	$^2P_{1/2}$	28	38.78	38.05	0.027	0.012	0.006	0.025
	$^4P_{1/2}$	30	38.69	37.96	0.027	0.013	0.011	0.037
	$^2D_{3/2}$	31	38.65	37.90	0.203	0.097	0.141	0.182
	$^4D_{5/2}$	32	38.48	37.72	0.005	0.003	0.001	0.007
	$^4S_{3/2}$	33	38.30	37.70	0.090	0.042	0.036	0.087
	$^4D_{3/2}$	34	38.37	37.57	0.083	0.037	0.027	0.098
	$^4D_{1/2}$	36	38.22	37.54	0.072	0.033	0.069	0.086
$5p^{-2}(^1D)6p$	$^2F_{5/2}$	39	37.40	37.00	0.017	0.010	0.009	0.016
	$^2P_{3/2}$	41	37.25	36.90	0.402	0.227	0.155	0.310
	$^2F_{7/2}$	42	37.27	36.85	0.326	0.365	0.328	0.300
	$^2D_{3/2}$	43	36.99	36.62	0.111	0.065	0.114	0.171
	$^2D_{5/2}$	44	36.98	36.59	0.199	0.121	0.127	0.194
	$^2P_{1/2}$	46	36.83	36.52	0.191	0.117	0.102	0.197
$5p^{-2}(^1S)6p$	$^2P_{1/2}$	65	35.24	34.60	0.000	0.000	0.000	0.000
	$^2P_{3/2}$	67,68	35.19	34.48	0.380	0.225	0.250	0.365
$5s^{-1}$	$^2S_{1/2}$	1	37.54	41.71	0.026	0.015	0.005	

[a]Reference [22].

TABLE IV. Calculated intensities (10^{-3} a.u.) for Xe $4d_{3/2}^{-1}6p$ Auger transitions (without multiplication by overlap intergals). FE is the same as in Table III. FEI is the same as FE, but ISCI was calculated using initial state orbitals. FE0 is the same as FE, but ISCI was omitted. The listed term is the leading LS term, which, due to a large mixing of the states, should be considered only as a tag of the transition.

Final ionic state		Initial state B				Initial state C			
Parent	Term	FE	FEI	FE0	Chen[a]	FE	FEI	FE0	Chen[a]
$5p^{-2}(^3P)6p$	$^4P_{3/2}$	0.019	0.030	0.030	0.065	0.012	0.002	0.002	0.005
	$^4P_{5/2}$	0.041	0.047	0.040	0.102	0.018	0.014	0.021	0.016
	$^2D_{5/2}$	0.020	0.025	0.033	0.024	0.035	0.031	0.024	0.077
	$^2S_{1/2}$	0.003	0.002	0.000	0.001	0.001	0.003	0.004	0.001
	$^4D_{7/2}$	0.029	0.107	0.000	0.016	0.019	0.038	0.049	0.057
	$^2P_{3/2}$	0.007	0.009	0.027	0.005	0.052	0.049	0.029	0.077
	$^2P_{1/2}$	0.000	0.001	0.003	0.003	0.004	0.003	0.001	0.006
	$^4P_{1/2}$	0.004	0.002	0.000	0.000	0.001	0.003	0.005	0.004
	$^2D_{3/2}$	0.031	0.055	0.060	0.133	0.030	0.008	0.003	0.020
	$^4D_{5/2}$	0.131	0.046	0.000	0.096	0.083	0.167	0.212	0.346
	$^4S_{3/2}$	0.048	0.028	0.006	0.024	0.006	0.025	0.046	0.065
	$^4D_{3/2}$	0.056	0.095	0.108	0.242	0.058	0.019	0.006	0.046
	$^4D_{1/2}$	0.015	0.011	0.003	0.009	0.001	0.006	0.014	0.006
$5p^{-2}(^1D)6p$	$^2F_{5/2}$	0.202	0.403	0.531	0.445	0.364	0.163	0.035	0.268
	$^2P_{3/2}$	0.125	0.151	0.177	0.397	0.170	0.147	0.124	0.259
	$^2F_{7/2}$	0.220	0.077	0.000	0.084	0.140	0.283	0.360	0.305
	$^2D_{3/2}$	0.194	0.307	0.347	0.435	0.207	0.096	0.056	0.143
	$^2D_{5/2}$	0.253	0.132	0.054	0.242	0.147	0.266	0.342	0.377
	$^2P_{1/2}$	0.076	0.023	0.000	0.082	0.056	0.106	0.127	0.185
$5p^{-2}(^1S)6p$	$^2P_{1/2}$	0.211	0.441	0.573	0.774	0.362	0.132	0.000	0.247
	$^2P_{3/2}$	0.309	0.092	0.004	0.160	0.260	0.476	0.562	0.827
$5s^{-1}$	$^2S_{1/2}$	0.013	0.013	0.010		0.003	0.003	0.007	

[a]Reference [22].

of 287 obtained using the GRASP computer code [21] indicates, as pointed out above, that the $4d_{3/2}^{-1}6p$ resonant Auger spectrum is entirely dominated by the transitions from the initial atomic state B of Table IV.

In the earlier calculations of Chen [22] and Fritzsche [23], not only the exchange interaction, but also the ISCI was completely ignored. Furthermore, no attention was paid to the population ratio of the two close lying initial states. The theoretical description for the $4d_{3/2}^{-1}$ transitions is thus considerably improved by our approach as compared with the previous calculations [22,23].

C. Shake-up transitions

The excited electron may shake to another orbital during the Auger decay due to the rearrangement of the ion core. The probability for a shake transition to occur during the decay is in the first approximation given by $P_{nn'} = |\langle nlj|n'lj\rangle|^2$. The $|n'lj\rangle$ in the overlap element is the orbital of an excited electron in the presence of the hole in the $n_il_ij_i$ subshell and $|nlj\rangle$ is the orbital which describes the excited electron in the field of the final core. For the resonant Auger decay in Xe, the $P_{6pn'}$ was obtained to be 0.801 ($n' = 6p$), 0.196 ($n' = 7p$), and 0.001 ($n' = 8p$). Therefore, the values of Table III should be multiplied by 0.801 to obtain the absolute partial rates of the spectator Auger transitions.

The final state effects cause differences in the spectral distribution of spectator and shake transitions. The energies and eigenvectors predicted by the MCDF calculations using the GRASP computer code [21] for the final states of both transitions differ remarkably from each other. The energy splitting is changed and also the mixing of the jj-coupled basis functions is altered in passing from the $5p^{-2}6p$ to $5p^{-2}np$ ($n \geq 7$) configuration. This is related to the change in the $5p$-np interaction which alters as a function of n. Further details will be discussed in a forthcoming paper dealing with the spectra taken at higher resonances.

The comparison not only between the spectator and shake transitions but also between them and the normal Auger transitions is of importance when the electron-electron interaction is considered. The Xe double-hole final states are intermediate coupling states, even if they are usually assigned with the LS symbols ^1S, ^1D, and ^3P. The $6p$-np electron induces a considerable mixing of these states. For example, the $5p^{-2}(^3P)np(^4D_{3/2})$, $5p^{-2}(^3P)np(^2P_{3/2})$, $5p^{-2}(^1D)np(^2P_{3/2})$, and $5p^{-2}(^1D)np(^2D_{3/2})$ states are strongly mixed, the mixing depending on the principal quantum number n. The changes in the mixing result in a redistribution of the intensity of the parent multiplets in passing from the normal Auger to the spectator and shake-up spectra.

IV. COMPARISON BETWEEN EXPERIMENT AND THEORY

A. The spectator Auger transitions

1. *Transition energies*

A comparison between the experimental and calculated energies is given in Table III for the $4d_{5/2}^{-1}6p \rightarrow 5p^{-2}6p$ transitions. The relative energies of the transitions are not very well reproduced by the MCDF calculations,

which include the FISCI as described above. The energy splitting is clearly overestimated when predicted by final state orbitals (Table III), but underestimated by initial state orbitals (not shown). The absolute ΔE_{SCF} energies differ by about 0.5 eV from the experimental ones. When the final state eigenvalues are calculated with the initial state orbitals, the absolute energies are in error by about 2 eV because the relaxation is omitted.

The discrepancies in the energy splitting between experiment and theory indicate that the inclusion of only the final state configurations of the resonant Auger transitions and the use of the average-level optimization scheme [21] do not properly reproduce the experiment. The strong interaction of the $(5s5p)^{-2}6p$ configuration with the $(5s5p)^{-2}7p$, $(5s5p)^{-2}4f$, and $(5s5p)^{-2}5f$ configurations reported in Ref. [16], but omitted in this work, most probably results in drastic changes in the eigenvectors and energies.

When fitting the $4d_{5/2}^{-1}6p \rightarrow 5p^{-2}6p$ deexcitation spectrum it was found that the line associated with the transition to the $5p^{-2}(^1S)6p(^2P_{3/2})$ state was clearly broader than 43 meV (FWHM) and could not be fitted by using only one line at 34.48-eV kinetic energy, which corresponds to the optical energy. This broadening cannot be explained by any enhanced satellite line or shake transition. Since the $5p^{-2}(^1S)6p(^2P_{3/2})$ state is below the double ionization threshold, the second step Auger decay is not allowed energetically. This rules out the possibility that the final state lifetime effects could cause the broadening of the line. Instead, it seems that the $5p^{-2}(^1S)6p(^2P_{3/2})$ final state is split into two almost equal components separated by about 20 meV from each other (lines 67 and 68 in Table I and Fig. 5). The corresponding components can be found also in the $4d_{3/2}^{-1}6p \rightarrow 5p^{-2}6p$ deexcitation spectrum. The finding is a clear indication of the strong interaction between the configurations, as discussed above.

2. The $4d_{5/2}^{-1}6p_{3/2}$ resonant Auger spectrum

A comparison with experiment shows that the distribution of the intensity between the fine structure components produced by the spectator-core coupling from the $5p^{-2}(^3P)$ parent line is fairly well reproduced by all the calculations. For most of the peaks the FE approach gives somewhat better agreement with experiment than the IE.

The discrepancy between experiment and theory is most noticeable in the case of the transitions to the $5p^{-2}(^1D)6p(^2F_{7/2})$ state (line 42 in Table II and Fig. 4). The F approximation overestimates the relative intensity of this line by a factor of 5, the overestimation being even larger (by a factor of 10) when the exchange interaction is included (FE). This transition is dominated by the $\epsilon g_{9/2}$ transition amplitude, which was found to be very sensitive to the exchange interaction. Relative intensities of the other components of the $5p^{-2}(^1D)$ parent are somewhat better reproduced in our calculations, even though the relative rates of the transition to the $5p^{-2}(^1D)6p(^2D_{3/2}$ and $^2P_{1/2})$ states (lines 43 and 46) are not correctly predicted by any of the models. The IE approximation gives a ratio of almost one for the transitions to the $^2D_{3/2}$ and $^2P_{1/2}$ components of the $5p^{-2}(^1D)$ parent, which clearly disagrees with the experimental spectrum. The transition to the $^2P_{1/2}$ is instead estimated to be the dominant one of these two transitions in both the F and FE calculations, in accordance with experiment. Exchange interaction has a minor effect on the branching ratio in most cases, indicating that the FISCI, influenced by the orbital set, plays the most prominent role.

The interaction between the $5p^{-2}6p$ and $5p^{-2}4f$ configurations was ignored in our calculations, which is why the intensity spread between the two lines at 34.48 eV (67 and 68 in Table II and Fig. 5) should be compared with the calculated relative intensity of the line corresponding to the $5p^{-2}(^1S)6p(^2P_{3/2})$ final state. All the calculations reproduce fairly well the experimental total intensity of the two lines.

In conclusion, the FE calculations give the best agreement with experiment, except for the transitions to the $5p^{-2}(^1D)6p(^2F_{7/2})$ state, which were found to be affected strongly by the exchange interaction. Since the additional FISCI influencing the transitions to the $5p^{-2}(^1S)6p(^2P_{3/2})$ state was ignored, the calculations do not reproduce the splitting of this line into two components.

3. The $4d_{3/2}^{-1}6p_{1/2,3/2}$ resonant Auger spectrum

The $4d_{3/2}^{-1}6p$ spectrum is entirely dominated by the transitions from the initial atomic state B of Table IV if the assumption that the photoexcitation branching ratio is properly reproduced by theory holds true. Partial rates obtained for this state in the FEI approximation seem to agree reasonably well with experiment. The branching ratios of the components of the $5p^{-2}(^1D)$ parent are better predicted by the FEI approach than by the FE or FE0. The FE0 approximation completely fails to reproduce the experiment, thus indicating that the inclusion of the ISCI is necessary. The finding that all the calculated intensity distributions associated with the initial state C differ clearly from the experimental one also supports the result that this state is not populated in the course of photoexcitation.

The ISCI and the population ratio of the initial states, completely omitted in earlier studies, clearly play an important role in the decay of the $4d_{3/2}^{-1}6p$ states. The capacity of the theoretical description to reproduce experiment is considerably improved by our calculations. The agreement with experiment is not complete, however, and further theoretical efforts are needed to clarify the source of the remaining discrepancy.

The disagreement between experiment and theory is most dramatic for close lying peaks that are now resolved using the Auger resonant Raman mode. The branching ratios of the components of the $5p^{-2}(^1D)$ parent thus provide a very sensitive test for theory. Moderate resolution would smear out all the fine structure and therefore give good overall agreement between experiment and theory.

B. Transitions to even-parity final states

The satellite lines associated with the $5s$ and $5p$ photoionization occur in the same energy region as the resonant Auger lines. The satellite spectrum is dominated by the even-parity configurations $5p^{-2}ns$ and $5p^{-2}nd$, which cannot admix with the final states of the resonant Auger decay due to their opposite parities. The participator Auger decay to the $5s^{-1}$ final state would populate the even-parity states due to the strong mixing between the $5s^{-1}$ and the $5p^{-2}ns$ and $5p^{-2}nd$ configurations. This may result in interferences which, from the theoretical point of view, do not strictly allow the separation of the transitions according to the parity of the final state. The participator Auger decay to the $5s^{-1}$ state is, however, estimated to be negligible, as can be seen from Tables III and IV, which show the partial rates of these transitions. This indicates that the interference effects should be small. On the other hand, the odd-parity final states $5p^4np$ were also found to be populated via direct photoionization, even though the population plays only a minor role in comparison with the deexcitation of the $4d^{-1}6p$ states.

The experimental results strongly support the assumption that the participator decay to even-parity final states is negligible. As stated in the Sec. II B, the decay of the $4d^{-1}6p$ excited states leads mainly to odd-parity final states. The even-parity final states show some changes in intensities, but their contribution to the total intensity enhancement is very small.

C. The normal Auger, spectator, and shake transitions

1. Shake contributions

Experimental and calculated energy shifts between the spectator and shake-up spectra are in reasonable agreement with each other. In the decay of the $4d_{5/2}^{-1}6p$ excitation the intensity ratio of the $7p$ shake and $6p$ spectator transitions is obtained to be 0.27:1 by experiment, which is in good agreement with the calculated value of 0.25. This indicates that the major contribution to the shake transitions is accounted for by the overlap matrix elements. The results are in accordance with earlier findings [2,24]. The decay of the $4d_{3/2}^{-1}6p$ state, on the other hand, shows an experimental shake contribution of 0.42 or 0.37, depending on whether the intensity of peak 66 is included or not, respectively. The fact that the theoretical shake predictions do not reproduce the observed differences in the shake probabilities between the $4d_{5/2}^{-1}$ and $4d_{3/2}^{-1}$ decay spectra is most probably connected to the FISCI. The $(5s5p)^{-2}7p$ and $(5s5p)^{-2}4f$ configurations are heavily mixed, preventing an unambiguous assignment of the final states. Further mixing with the $(5s5p)^{-2}6p$ configuration makes it even more difficult to divide the peaks into the spectator or shake-up transitions. Peak 66, which is assigned as a shake-up line in the $4d_{3/2}^{-1}$ spectrum but not even observed in the $4d_{5/2}^{-1}$ spectrum, serves as a good example here, even though the interpretation of some other less intense peaks may also suffer from the strong mixing of the configurations.

2. Evolution of the intensity of parent multiplets

A comparison between the spectator, shake-up, and also the normal Auger spectra makes it possible to see how dramatic the changes are in the electron-electron interaction. The experimental results display a clear redistribution of the intensity of the parent multiplets in passing from the normal Auger to the spectator and to the shake-up spectra.

The relative intensities of the ^3P, ^1D, and ^1S parent multiplets obtained by experiment and theory are given in Table V for the $4d_{5/2}^{-1}$ and $4d_{3/2}^{-1}$ normal, resonant Auger, and shake-up spectra. The ^1D parent line clearly gains strength on passing from the $4d_{5/2}^{-1}$ normal to the spectator Auger decay. The effect is also evident but less pronounced in the case of the $4d_{3/2}^{-1}$ transitions. The FE and IE calculations reproduce the tendency of the changes, even though they fail to predict the branching ratios perfectly. The branching ratios are very sensitive to the mixing of the parent states. The parent mixing is further disturbed via the mixing with other configurations of same parity. An unambiguous assignment of the lines is therefore difficult; hence the branching ratios of shake-up lines have especially large uncertainties.

Note that the intensity distributions of the $4d_{3/2}^{-1}$ and $4d_{5/2}^{-1}$ transitions differ remarkably from each other in both the normal and resonant Auger spectra. Also the intensity distribution between the fine structures produced by the spectator-core coupling differ remarkably, as can be seen from Figs. 2–7. The differences are nicely reproduced by the MCDF calculations, which fully account for the relativistic effects.

3. Electron correlation beyond the present MCDF calculations

Although the overall agreement between experiment and theory is good, the remaining discrepancies indi-

TABLE V. Branching ratio of parent lines.

State	Method	^3P	^1D	^1S
		spectator		
$4d_{5/2}^{-1}$	expt.	44.3	40.4	15.3
	calc. FE/IE	34.7/39.7	52.3/46.4	13.0/13.9
$4d_{3/2}^{-1}$	expt.	19.0	54.8	26.2
	calc. FE	20.3	53.7	26.1
		normal		
$4d_{5/2}^{-1}$	expt.	46.4	32.2	21.4
	calc. FE/IE	38.9/40.1	46.7/45.4	14.4/14.5
$4d_{3/2}^{-1}$	expt.	12.9	46.4	40.8
	calc. FE/IE	18.3/18.7	53.0/52.1	28.7/29.1
		shake-up		
$4d_{5/2}^{-1}$	expt.	41.6	43.2	15.2
$4d_{3/2}^{-1}$	expt.[a]	41.4/34.6	41.4/46.2	17.2/19.2

[a]Including/not including line 66.

cate that the many-electron correlation effects, ignored in present calculations, play an important role. Experimental ratios of the Xe normal Auger lines were found to be somewhat better described by the multichannel multiconfiguration Dirac-Fock results [20,25], which take the mixing of continuum channels into account. This indicates that the channel mixing, omitted in present calculations, is important in the case of resonant Auger transitions as well. The effect might be even stronger in the case of resonant Auger decay due to the near degeneracy of several configurations allowing for a pronounced FISCI and channel mixing.

In the comparison with experiment, the discrepancies may be addressed not only to those correlation effects that were not included in the calculation of the transition amplitudes, but also to the incomplete treatment of the orthogonality in our FEI approximation. The *ab initio* approach to overcome this imperfection would be to determine the orbitals and mixing coefficients for the initial and final states in separate SCF calculations and to include the correlation terms coming from the nonorthogonality of the one-electron orbitals in the transition amplitudes. Such a procedure was found, however, to alter the branching ratios of the normal Auger lines of Xe only slightly [25].

In this work we have assumed a two-step description of the Auger effect and neglected the direct photoionization channels. Our experiment indicates that the interference effects between the participator Auger channel and the photoionization channel are small. The two-step formulation seems to be adequate in describing the excitation and the subsequent decay of the excited state.

V. CONCLUSIONS

By utilizing the Auger resonant Raman effect the lifetime broadening has been eliminated in the Xe $4d^{-1}6p$ resonant Auger spectra. This has made it possible to determine the relative intensities of the separate resonant Auger transitions with an accuracy that made a detailed comparison with theory possible. Moderate resolution would smear out the detailed fine structure, making it impossible to test whether the partial transition rates are correctly reproduced by theory.

The FEI approximation, accounting for the exchange interaction as well as the ISCI and FISCI effects, was found to give the best agreement with experiment. The results, however, clearly indicate that correlation effects, beyond the present MCDF calculations, play a prominent role in the resonant Auger decay.

ACKNOWLEDGMENTS

We are grateful to the staff of Max-laboratory for assistance and cooperation during the measurements. Financial support from the Research Council for Natural Sciences of the Academy of Finland, the Swedish Natural Science Research Council (NFR), and the Royal Swedish Academy of Sciences is acknowledged.

[1] W. Eberhardt, G. Kalkoffen, and C. Kunz, Phys. Rev. Lett. **41**, 156 (1978).

[2] H. Aksela, S. Aksela, J. Tulkki, T. Åberg, G. M. Bancroft, and K. H. Tan, Phys. Rev. A **39**, 3401 (1989); H. Aksela, S. Aksela, H. Pulkkinen, G. M. Bancroft, and K. H. Tan, *ibid.* **37**, 1798 (1988); H. Aksela, S. Aksela, A. Mäntykenttä, J. Tulkki, E. Shigemasa, A. Yagishita, and Y. Furusawa, Phys. Scr. **T41**, 113 (1992), and references therein.

[3] S. B. Whitfield, C. D. Caldwell, D. X. Huang, and M. O. Krause, J. Phys. B **25**, 4755 (1992).

[4] T. A. Carlson, D. R. Mullins, C. E. Beall, B. W. Yates, J. W. Taylor, D. W. Lindle, and F. A. Grimm, Phys. Rev. A **39**, 1170 (1989).

[5] H. Aksela, G. M. Bancroft, and B. Olsson, Phys. Rev. A **46**, 1345 (1992).

[6] H. Aksela, S. Aksela, O.-P. Sairanen, A. Kivimäki, A. Naves de Brito, E. Nõmmiste, J. Tulkki, S. Svensson, A. Ausmees, and S. J. Osborne, Phys. Rev. A **49**, R4269 (1994).

[7] G. S. Brown, M. H. Chen, B. Crasemann, and G. E. Ice, Phys Rev. Lett. **45**, 1937 (1980); G. B. Armen, T. Åberg, J. C. Levin, B. Crasemann, M. H. Chen, G. E. Ice, and G. S. Brown, *ibid.* **54**, 1142 (1985).

[8] A. Kivimäki, A. Naves de Brito, S. Aksela, H. Aksela, O.-P. Sairanen, A. Ausmees, S. J. Osborne, L. B. Dantas, and S. Svensson, Phys. Rev. Lett. **71**, 4307 (1993).

[9] J. Tulkki, H. Aksela, and N. M. Kabachnik, Phys. Rev. A **50**, 2366 (1994).

[10] S. Aksela, A. Kivimäki, A. Naves de Brito, O.-P. Sairanen, S. Svensson, and J. Väyrynen, Rev. Sci. Instrum. **65**, 831 (1994).

[11] R. Nyholm, S. Svensson, J. Nordgren, and A. Flodström, Nucl. Instrum. Methods A **246**, 267 (1986); S. Aksela, A. Kivimäki, R. Nyholm, and S. Svensson, Rev. Sci. Instrum. **63**, 1252 (1992).

[12] S. J. Osborne, A. Ausmees, J. O. Forsell, B. Wannberg, G. Bray, L. B. Dantas, S. Svensson, A. Naves de Brito, A. Kivimäki, and S. Aksela, Synchr. Rad. News **7**(1), 25 (1994).

[13] B. Kämmerling and V. Schmidt, J. Phys. **26**, 1141 (1993).

[14] M. O. Krause, S. B. Whitfield, C. D. Caldwell, J.-Z. Wu, P. van der Neulen, C. A. de Lange, and R. W. C. Hansen, J. Electron Spectrosc. Relat. Phenom. **58**, 79 (1992).

[15] G. C. King, M. Tronc, F. H. Read, and R. C. Bradford, J. Phys. B **10**, 2479 (1977).

[16] J. E. Hansen and W. Persson, Phys. Scr. **36**, 602 (1987).

[17] J. Jauhiainen, A. Ausmees, A. Kivimäki, S. J. Osborne, A. Naves de Brito, S. Aksela, S. Svensson, and H. Aksela, J. Electron Spectrosc. Relat. Phenom. **69**, 181 (1994).

[18] M. Carlsson-Göthe, P. Baltzer, and B. Wannberg, J. Phys. B **24**, 2477 (1991).

[19] J. Tulkki, T. Åberg, A. Mäntykenttä, and H. Aksela, Phys. Rev. A **46**, 1357 (1992).

[20] J. Tulkki, N. Kabachnik, and H. Aksela, Phys. Rev. A **48**, 1277 (1993).

[21] K. G. Dyall, I. P. Grant, C. T. Johnson, F. A. Parpia, and E. P. Plummer, Comput. Phys. Commun. **55**, 425 (1989).
[22] M. H. Chen, Phys. Rev. A **47**, 3733 (1993).
[23] S. Fritzsche, Phys. Lett. A **180**, 262 (1993).
[24] H. Aksela, S. Aksela, H. Pulkkinen, A. Kivimäki, and O.-P. Sairanen, Phys. Scr. **41**, 425 (1990).
[25] A. Mäntykenttä, Phys. Rev. A **47**, 3961 (1993).